Diocotron Instability in Plasmas and Gas Discharges

Cite as: Journal of Applied Physics **37**, 602 (1966); https://doi.org/10.1063/1.1708223
Submitted: 29 April 1965 . Published Online: 17 June 2004

W. Knauer

Diocotron Instability in Plasmas and Gas Discharges

W. KNAUER
Hughes Research Laboratories, Malibu, California
(Received 29 April 1965)

The wave interaction underlying the diocotron effect is re-examined and a physical model of the instability presented. A wave analysis is then given for circular, wall-enclosed charge layers with finite length in the axial direction. Circular layers are of particular interest, since they apply to various plasma, discharge, and electron device geometries. Their instability behavior is found to be similar in many respects to the behavior of linear charge sheets, described in earlier work by R. W. Gould. In contrast to linear sheets, however, circular layers are unstable only when their thickness is sufficiently small. This effect is associated with the inability of charge perturbations to have a wavelength which exceeds the layer circumference. Data are presented for the magnitude of growth in various configurations and for the critical layer width at which growth terminates.

I. INTRODUCTION

THE "diocotron effect" or "slipping stream instability" occurs in unneutralized charge sheets of finite width in the presence of a magnetic field. The term "diocotron effect" has been coined to indicate that the sheet charges must "give chase," or more precisely, must slip parallel to the sheet surface to create the instability. Such a slip can result when the charges are subjected to the space-charge fields of the sheet as well as to a suitably applied magnetic field. With a magnetic field directed into the depth of the sheet, the charges carry our $\mathbf{E}\times\mathbf{B}$ drifts parallel along the sheet. Since the intensity of the space-charge field increases across the sheet, the magnitude of the drift varies accordingly and the sheet slips.

The instability itself is the result of an interaction between two waves which propagate along the sheet surfaces. These waves resemble water surface waves in many respects. Unlike water waves, however, they can propagate in only one direction. Waves at the upper and lower sheet surfaces must propagate in opposite directions. Since propagation is relative to the motion of the surface charges, the slip from surface to surface affects the velocity with which waves at the upper and lower surfaces meet. Generally, the slip tends to slow down the rate of encounter and, under suitable conditions, the two waves can be halted completely. Mutual interaction then produces a single, exponentially growing wave mode.

Discovery of this phenomenon dates back to a wartime study of electron dynamics in magnetrons by Buneman.[1] Analytic descriptions of the instability have been given by Buneman,[2] McFarlane, and Hay,[3] Gould,[4,5] Kyhl and Webster,[6] and by Pierce.[7] While these presentations concern the same basic configuration—a flat charge sheet—they cover different ratios of plasma to cyclotron frequencies. The general treatment for arbitrary ratios ω_p/ω_c is analytically very involved and has not been accomplished to date. McFarlane and Hay have been able to solve the special case $\omega_p/\omega_c=1$. Gould later provided solutions under the assumption $\omega_p/\omega_c\ll 1$, which includes many situations of interest. Finally, Kyhl and Webster, as well as Pierce, have treated the case of arbitrary ω_p/ω_c in the limit of small sheet widths.

Few of the charge layers in actual crossed field configurations can be analyzed satisfactorily in terms of flat charge sheets in free space. Most of these layers in plasmas, discharges, and electron devices are of circular geometry and are enclosed by walls. Magnetically confined plasma columns, for example, comprise unneutralized sheaths, which are subjected to radial space charge fields and to an axial magnetic field. These sheaths are of cylindrical shape and are usually surrounded by walls. Reflex discharges also contain circular charge layers. Electrons trapped by the axial magnetic field accumulate inside the anode cylinder to form an unneutralized, cylindrical charge layer.

Among other crossed field configurations which comprise unneutralized charge layers are some of the experimental thermonuclear plasma devices, notably the E layer of the Astron and homopolar plasmas. In addition, the charge layer of a recently proposed space-charge radiation shield for space vehicles,[8] which surrounds the spacecraft and which is magnetically confined, falls into this category. The rotating cloud of a magnetron finally is the classical example for a charge layer subjected to crossed fields. Actually, the familiar magnetron instability results from an interaction between electron cloud and anode circuit and hence is different from the diocotron effect. Nevertheless, the diocotron instability may play a role in the conditions for current cutoff and for oscillation onset in magnetrons.

All configurations mentioned above have in common circular charge layers, and, for this geometry, the

[1] O. Buneman, C. V. D. Report Mag. 37 (1944), also J. Electronics 3, 1 (1957).
[2] O. Buneman, J. Electron. Control 3, 507 (1957).
[3] G. G. McFarlane and H. G. Hay, Proc. Phys. Soc. (London) B63, 409 (1950).
[4] R. W. Gould, California Institute of Technology Electron Tube and Microwave Laboratory Tech. Report No. 3 (1955).
[5] R. W. Gould, J. Appl. Phys. 28, 599 (1957).
[6] R. L. Kyhl and H. F. Webster, IRE Trans. Electron Devices ED-3, 172 (1956).
[7] J. R. Pierce, IRE Trans. Electron Devices ED-3, 183 (1956).
[8] R. H. Levy, paper presented at 6th Annual Meeting of Plasma Physics Division of APS, New York, November 1964.

question of stability has not yet been discussed. Accordingly, it is the objective of this paper to provide an instability analysis for cylindrical charge sheets, in which the effect of surrounding walls is taken into account.

II. BASIC PROPERTIES OF DIOCOTRON EFFECT

The diocotron effect belongs to a group of wave modes in charged particle ensembles where space-charge fields and the magnetic field furnish the driving forces. In deriving these waves, a quasistatic approach is permissible, leading to the customary condition

$$\nabla \times \mathbf{E}=0. \tag{1}$$

The wave analysis generally includes Poisson's equation (in cgs units)

$$\nabla \cdot \mathbf{E}=4\pi\rho, \tag{2}$$

the equation of continuity

$$(\partial\rho/\partial t)+\nabla(\rho_0\mathbf{v}+\rho\mathbf{u})=0, \tag{3}$$

and the equation of motion

$$\frac{d\mathbf{v}}{dt}=\frac{e}{m}\left[\mathbf{E}+\frac{1}{c}(\mathbf{v}\times\mathbf{B})\right], \tag{4}$$

Here, $\mathbf{u}$ and ρ_0 are the unperturbed, $\mathbf{v}$ and ρ the perturbed velocities and densities. $\mathbf{E}$ is the perturbation field. By suitable choice of initial and boundary conditions, Eqs. (1) to (4) can be solved to yield the diocotron instability. Before approaching solutions for circular configurations, a straightforward derivation of the known solution for a flat charge sheet is given to shed light upon the physical nature of the instability.

First, waves are considered which propagate inside and along the surface of an ensemble filling the half space. The ensemble is assumed to be of density ρ_0, unneutralized, and subjected to a magnetic field $\mathbf{B}$ [see Fig. 1(a)]. The direction of wave propagation is taken to be transverse with respect to $\mathbf{B}$, and the wave amplitude to be independent of distance along $\mathbf{B}$. Following Gould's analysis, Eqs. (1) and (4) can be combined to provide a field equation. If the time-dependent quantities E_y, E_x, v_y, v_x, and ρ vary as $\exp[j(\omega t-\beta x)]$, Eqs. (1) and (2) can be expressed as

$$\partial^2E_x/\partial y^2-\beta^2E_x=-j\beta 4\pi\rho. \tag{5}$$

Similarly, Eq. (3) becomes

$$\rho=j\rho_0\frac{\partial v_y/\partial y-j\beta v_x}{\omega-\beta u}, \tag{6}$$

and (4) becomes

$$\begin{aligned} v_y&=-(e/m)(1/\Omega^2)[j(\omega-\beta u)E_y-\omega_cE_x],\\ v_x&=-(e/m)(1/\Omega^2)[j(\omega-\beta u)E_x+(\omega_c-\Delta)E_y], \end{aligned} \tag{7}$$

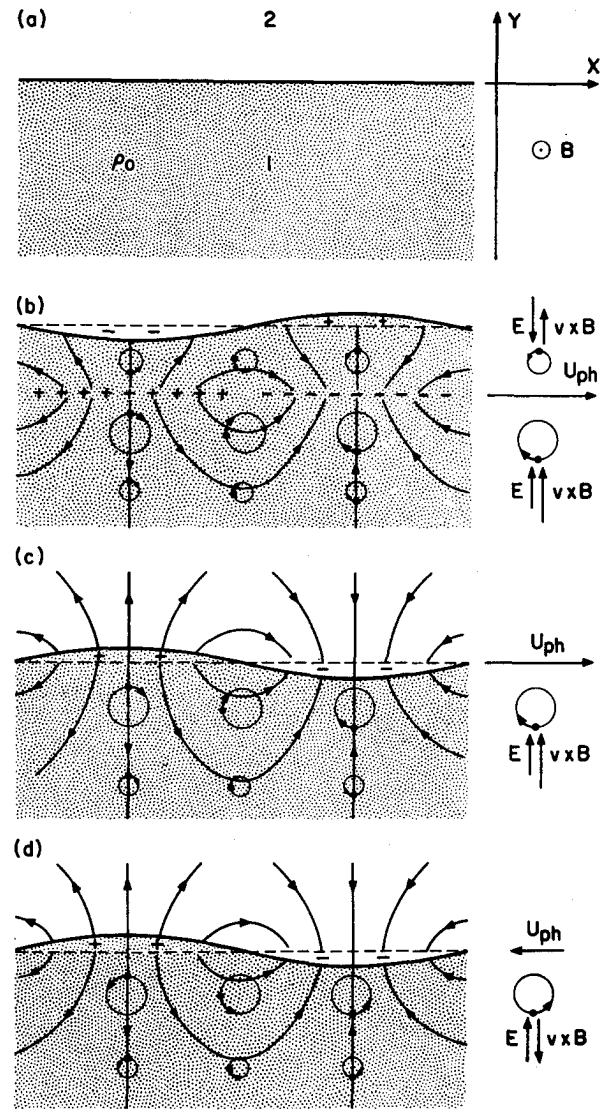

FIG. 1. Crossed field waves in a charge ensemble, filling the half-space. (a) Unperturbed configuration, (b) example of a volume wave mode, (c) "fast" surface wave mode, (d) "slow" surface wave mode.

where u is the velocity slip in the x direction, Δ is the gradient of u in the y direction:

$$\Delta\equiv\partial u/\partial y=\omega_p^2/\omega_c, \tag{8}$$

and $\Omega^2=(\omega-\beta u)^2-\omega_c(\omega_c-\Delta)$. Equations (5) to (7) yield the basic field equation

$$\left(1-\frac{\omega_p^2}{\Omega^2}\right)\left(\frac{\partial^2E_x}{\partial y^2}-\beta^2E_x\right)-2\frac{\omega_p^2\omega_c}{\Omega^4}\Delta\left(\frac{\omega-\beta\mu}{\omega_c}\beta\frac{\partial E_x}{\partial y}+\beta^2E_x\right)=0. \tag{9}$$

Unfortunately, the general solution to this equation is not known. Gould derived a special solution for the

case where the charges are neutralized. With $\Delta=0$, Eq. (9) becomes

$$[(\omega-\beta u)^2-(\omega_p^2+\omega_c^2)]\left(\frac{\partial^2 E_x}{\partial y^2}-\beta^2 E_x\right)=0. \quad (10)$$

Equation (10) is valid for arbitrary ratios of ω_p/ω_c and has three types of solutions. The first of these derives from

$$(\omega-\beta u)^2=\omega_p^2+\omega_c^2 \quad (11)$$

and comprises various oscillations and waves which are confined to the interior of the ensemble. The wave mechanism in one specific wave mode of this type is illustrated in Fig. 1(b). It has been assumed here that a sinusoidal density modulation is imposed upon a single, infinitesimally thin charge layer along the x direction. In a frame of reference in which the ensemble is at rest ($u=0$), all charges move circularly at the hybrid frequency $(\omega_p^2+\omega_c^2)^{\frac{1}{2}}$ under the combined electric and magnetic field forces. The orbits on one side of the excited layer are generally much smaller than those on the other; this is because electric and magnetic forces are opposed on one side while on the other they are directed in parallel [see Fig. 1(b)].

The other types of waves are associated with

$$(\partial^2 E_x/\partial y^2)-\beta^2 E_x=0. \quad (12)$$

Equation (12) is identical to the free space field equation and hence the charge density within the ensemble must remain unperturbed. The sheet thus has the property of an incompressible fluid, and perturbations can occur only at the surface. For an ac surface charge density, varying as $\exp[j(\omega t-\beta x)]$, Eq. (12) yields exponentially decaying fields which, below the surface, can be expressed as

$$E_{y1}=C_1 e^{\beta y},$$
$$E_{x1}=-jC_1 e^{\beta y}, \quad (13)$$

and above as

$$E_{y2}=C_2 e^{-\beta y}, \quad (14)$$
$$E_{x2}=jC_2 e^{-\beta y}.$$

At the surface itself, the fields from both sides have to match in accordance with

$$E_{y2}|_s=E_{y1}|_s+4\pi\sigma,$$
$$E_{x2}|_s=E_{x1}|_s, \quad (15)$$

where σ is the ac surface density. In addition, continuity of charge flow across the surface requires that

$$d\sigma/dt\equiv j(\omega-\beta u)\sigma=\rho_0 v_y. \quad (16)$$

If (7) is introduced into (16) (with $\Delta=0$) and if (13) to (16) are combined, the following dispersion relation obtains:

$$\omega-\beta u=\tfrac{1}{2}\omega_c\pm\tfrac{1}{2}(\omega_c^2+2\omega_p^2)^{\frac{1}{2}}. \quad (17)$$

Equation (17) describes two surface waves. Figure 1(c) illustrates the mechanism of the wave associated with the plus sign. This "fast" wave is closely related to the volume wave of (11), as can be seen from the identical particle orbits in both cases. The difference in oscillation frequency can be attributed to the presence of additional charges above the excited layer in the case of the volume wave.

The negative sign in (17) leads to a slowly propagating surface wave, the mechanism of which is shown in Fig. 1(d). In contrast to the "fast" wave case, where electric and magnetic field forces are oriented in parallel, here the forces oppose each other, resulting in a relatively slow rotational motion and thus in slow propagation. The condition of the latter type of wave becomes particularly clear when $\omega_p/\omega_c\ll 1$. In this limit, the dispersion equation (17) reduces to

$$\omega-\beta u=-\tfrac{1}{2}\omega_p^2/\omega_c. \quad (19)$$

If (19) is now introduced into (7), a simplified set of equations of motion obtains:

$$v_y=-(E_x/B)c, \quad v_x=(E_y/B)c. \quad (20)$$

According to (20), the particle motion then consists solely of $\mathbf{E}\times\mathbf{B}$ drifts. Dynamically, this means that the opposing electric and magnetic field forces are exactly equal.

The motion pattern in both types of surface waves is much like the motion of water molecules in an infinitely deep body of water when a surface wave is present. Water molecules and charges alike perform circular motions (in the rest frame of the charge ensemble where $u=0$) in which the circle diameters decrease exponentially with distance from the surface. This equivalence extends even to configurations of finite depth. In both cases, the trajectories then become ellipses. At the bottom, the orbits degenerate into linear oscillations, extending parallel to the bottom surface. In the space-charge wave case, the bottom must be conductive so that this motion pattern will prevail. In the absence of a conductive bottom, the charge ensemble has a second free surface and two additional surface waves can arise. It is seen that the interaction between the "slow" waves of the two surfaces leads to the diocotron instability, when a velocity slip is present.

For a convenient description of this interaction, one may choose a frame of reference in which the center layer of the slipping sheet is at rest [see Fig. 2(a)]. Since this frame is symmetrical with respect to the two interacting surface waves, the resultant growing wave mode can be expected to be stationary. Its variation in time and space must then be expressible as $\exp(\alpha t-j\beta x)$, where α is the growth rate.

Basically the instability is treated in the limit $\omega_p/\omega_c\ll 1$ and is regarded as an interaction between two surface waves of the type given by (19). It is assumed that the amplitudes of both waves are the same and that the charge motion in each is modified by the elec-

trostatic fields of the other. The surface charge σ of wave 1 at the lower surface ($\sigma=\sigma_1=\sigma_2$) generates the field components

$$E_{y12}=2\pi\sigma e^{-\beta t},$$
$$E_{x12}=j2\pi\sigma e^{-\beta t}, \tag{21}$$

at the upper surface. The x component of the electric field produces a y directed drift

$$v_{y12}=-j2\pi\sigma(c/B)e^{-\beta t}. \tag{22}$$

This leads to the following flow of charge across the upper surface

$$d\sigma_{12}/dt=v_{y12}\rho_0=-j\tfrac{1}{2}(\omega_p^2/\omega_c)\sigma e^{-\beta t}. \tag{23}$$

In addition, wave 2 at the upper surface generates its own flow. By itself, wave 2 propagates as $\exp[j(\omega t-\beta x)]$ where ω and β are related by (19). The latter equation remains valid even in the presence of slip, since in the limit $\omega_p/\omega_c\ll 1$ both the equation of motion (20) and the field equation (12) remain unchanged. Hence, the charge flow associated with wave 2 is

$$d\sigma_{22}/dt=j(\omega-\beta u_2)\sigma. \tag{24}$$

Here u_2 represents the velocity slip at the upper surface, which, according to (8) is

$$u_2=(\omega_p^2/\omega_c)\tfrac{1}{2}t. \tag{25}$$

The total charge flow across the upper surface then becomes

$$d\sigma_2/dt=-\tfrac{1}{2}j(\omega_p^2/\omega_c)\{1+[\delta+j(1-\delta^2)^{\frac{1}{2}}]e^{-\beta t}\}\sigma, \tag{26}$$

where the expression in brackets [ ] accounts for a possible phase difference between both wave components ($-1\leqq\delta\leqq+1$).

Existence of a single, growing wave requires that

$$d\sigma_2/dt=(\alpha-j\beta u_2)\sigma=[\alpha-\tfrac{1}{2}j(\omega_p^2/\omega_c)\beta t]\sigma. \tag{27}$$

Combination of (26) and (27) yields the dispersion equation

$$\alpha-\tfrac{1}{2}j(\omega_p^2/\omega_c)\beta t = -\tfrac{1}{2}j(\omega_p^2/\omega_c)\{1+[\delta+j(1-\delta^2)^{\frac{1}{2}}]e^{-\beta t}\}. \tag{28}$$

The imaginary portion of this relation determines the phase factor

$$\delta=(\beta t-1)e^{\beta t}. \tag{29}$$

Introduction of δ into the real part of (28) finally yields the growth rate

$$\alpha=\pm\tfrac{1}{2}(\omega_p^2/\omega_c)[e^{-2\beta t}-(\beta t-1)^2]^{\frac{1}{2}}. \tag{30}$$

This expression is identical to one derived by Gould,[4] except for a factor which is accounted for by the different frame of reference.

According to (30), the growth rate first increases linearly with sheet width, reaches a maximum, and eventually falls back to zero at $\beta t\cong 1.3$. This dependence can be explained as follows. Without mutual interaction,

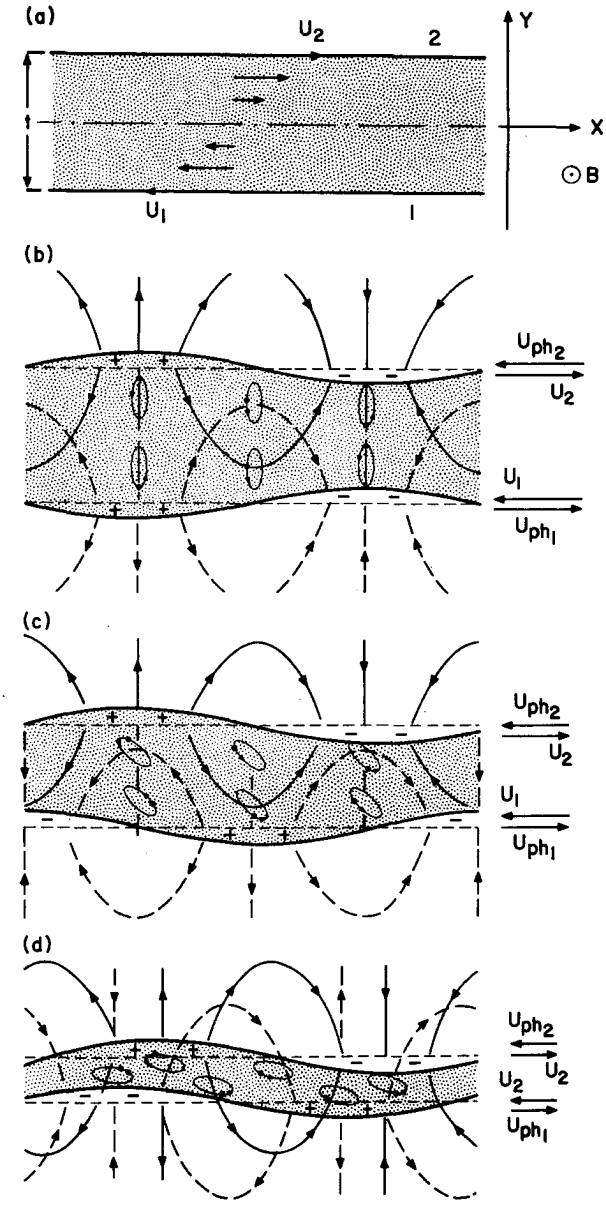

FIG. 2. Diocotron effect in a linear charge sheet of finite width. (a) Unperturbed configuration, (b) sausage-like perturbation in a thick sheet with $\beta t=1.3$ (drawing not to scale), (c) combination of sausage and meander-like perturbations in a sheet of medium width ($\beta t=1$), (d) predominantly meander-like perturbation in a thin sheet ($\beta t=0.5$).

the upper and lower surface waves would propagate as $\exp[j(\omega t\pm\beta x)]$ or, in terms of the phase velocity, as

$$u_{\rm ph}=\pm\tfrac{1}{2}(\omega_p^2/\omega_c)(\beta t-1). \tag{31}$$

Thus, only for $\beta t=1$ would both waves automatically be synchronized with each other. For all other values of βt, synchronization can be achieved only by interaction. Clearly, this takes place at the cost of growth. The proper amount of interaction is provided by suitable adjustment of the phase angle between both waves (see Fig. 2). At $\beta t=0$ and $\beta t\cong 1.3$ the relative phase

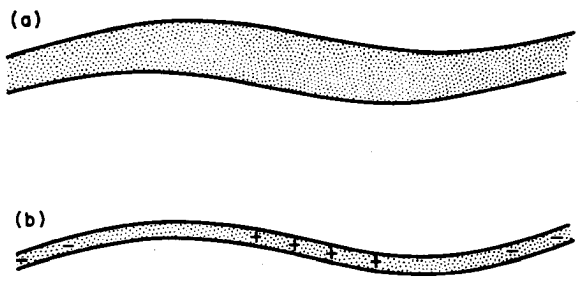

FIG. 3. Comparison of the perturbed thin beam configuration treated by Gould[3] and in this paper with the configurations discussed by Kyhl and Webster,[5] by Pierce,[6] and by Gould.[4] In the limit of zero sheet width both have the same ac field configurations.

angles are zero ($\delta=-1$) and π ($\delta=+1$), respectively. Here, both waves tend to move fast against each other and since both have to apply themselves fully to synchronization, the growth rate is zero. For values of βt closer to $\beta t=1$, less interaction is required for synchronization and more growth can take place. At $\beta t=1$, the phase angle is $\frac{1}{2}\pi$ ($\delta=0$) and the interaction fully benefits growth. Actually, the maximum growth rate does not occur at $\beta t=1$, but at $\beta t\cong 0.8$ where a stronger interaction because of larger fields at the shorter distance outweighs a less favorable phase angle. Finally, for $\beta t>1.3$, the interaction between the two waves becomes too weak to make synchronization possible and both modes must propagate separately.

As can be seen from Fig. 2, the diocotron effect produces meander or sausage shaped distortions, depending upon whether the sheet is thin or thick. At intermediate widths, the distortion is a combination of both. In all cases the charge density within the sheet volume remains unchanged. This is in apparent contradiction to several independent thin sheet analyses carried out by Kyhl and Webster,[6] Pierce,[7] and Gould.[5] In these analyses it has been assumed that a thin sheet with negligibly small slip has a meander-like shape distortion and at the same time carries a sinusoidal density perturbation. The growth rate of such a configuration turns out to be identical with the rate given by (30) when taken in the limit of small βt. This suggests that in both analyses the same interaction is treated. Figure 3 shows that this is actually so; it illustrates that in the limit of a thin sheet, the ac fields of a slipping stream with shape distortion are identical to those of a very thin meandering sheet with superimposed density perturbation.

For completeness it appears desirable to consider the possibility of other unstable interactions among the three different types of wave modes described earlier. In the case of a neutralized, and hence nonslipping sheet of finite width, Gould has found two "slow" and two "fast" surface waves and an infinite number of volume waves, all of which are propagating. The lack of growth is immediately obvious from the dispersion diagram shown in Fig. 4. Here the dispersion curves for the different wave modes do not cross.

The situation in a slipping sheet of finite width is considerably more complicated. Since the dispersion equation for this case has not been determined, the discussion must remain somewhat vague. The special case $\omega_p/\omega_c=1$, treated by McFarlane and Hay, has led to a solution with three unstable wave modes. One of these is the diocotron mode; the two others can be identified as interactions between one "slow" surface wave and one volume wave.

An approximate dispersion diagram for this situation is obtained simply by assuming that a slipping charge sheet supports the same type of wave modes as the nonslipping sheet and that propagation takes place relative to the velocity of the excited charge layer. The resulting ω–β diagram (see Fig. 5) includes three crossovers between waves which agree closely with the three unstable modes predicted by McFarlane and Hay.

For $\omega_p/\omega_c=1$, all three unstable wave modes involve a modulation of the volume density of the sheet, as can be seen from (9). If ω_p/ω_c is decreased, this density modulation vanishes rapidly in the case of the "slow" wave, since (9) converts into the free space equation (12) for $\omega\cong\omega_p^2/\omega_c$. This has an important consequence for the two surface-volume wave interactions. If they are to produce growth, the wave components must interact constructively with each other. Fields of the volume wave have to enhance the ac surface charge, and fields of the surface wave have to enhance the volume ac density. However, since for $\omega_p/\omega_c\ll 1$ the surface wave is governed by the free space equation, it cannot produce any ac charge density modulation within the sheet. Hence, in the limit $\omega_p/\omega_c\ll 1$, the two surface–volume wave interactions cease to produce growth. Since (9) approaches the free space Eq. (12) as $(\omega_p/\omega_c)^4$, lack of growth should extend very closely

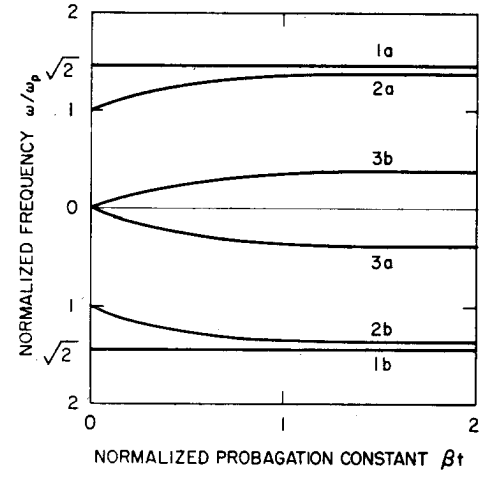

FIG. 4. Dispersion diagram of a nonslipping sheet of finite width ($\omega_p/\omega_c=1$). The absence of crossovers between different modes suggests that an instability does not exist. Modes 1(a) and 1(b) are the volume waves described by Eq. (11). Modes 2(a) and 2(b) are the upper and lower "fast" surface waves and modes 3(a) and 3(b) are the lower and upper "slow" surface waves.

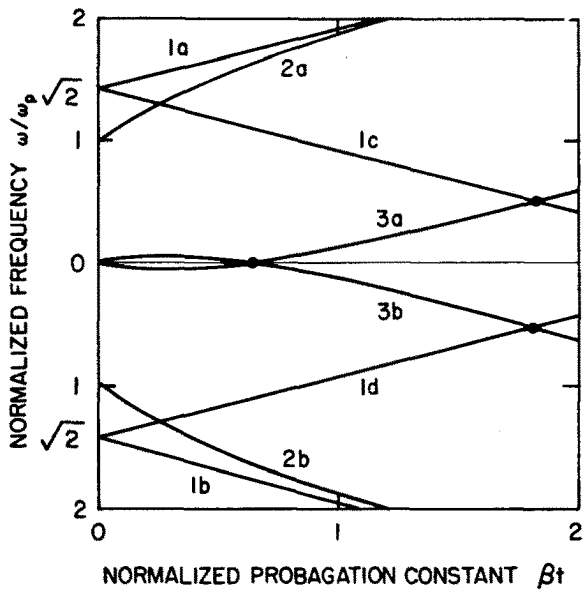

FIG. 5. Approximate dispersion diagram for a slipping sheet of finite width ($\omega_p/\omega_c=1$). The diagram was obtained under the assumption that aside from a superimposed velocity slip, the wave modes are the same as those in a nonslipping sheet. Modes 1(a) and 1(b) are volume waves with an excited charge layer near the upper surface; modes 1(c) and 1(d) are volume waves associated with a similar layer near the lower surface. Modes 2(a) and 2(b) are "fast" surface waves, modes 3(a) and 3(b) are "slow" surface waves. The circled intersections coincide with the unstable modes found by McFarlane and Hay.[2]

up to $\omega_p/\omega_c=1$. Conversely, a treatment of the diocotron interaction, using the free space Eq. (12), should be valid to values of ω_p/ω_c which closely approach unity.

III. DIOCOTRON EFFECT IN CIRCULAR GEOMETRIES

The instability of a circular sheet of finite length, as shown in Fig. 6, is discussed in this section. Equations (1) to (4) can best be solved for the ac potential ϕ. Under the assumption that ϕ varies as $\exp[j(\omega t-n\theta-kz)]$, Trivelpiece and Gould[9] have derived the differential equation

$$\frac{1}{r}\frac{\partial}{\partial r}\left(r\frac{\partial\phi}{\partial r}\right)-\frac{n^2}{r^2}\phi-T^2\phi=0, \tag{32}$$

where

$$T=-k^2\frac{1-\omega_p^2/\omega^2}{1+[\omega_p^2/(\omega_c^2-\omega^2)]}. \tag{33}$$

Generally, the solutions to (32) can be expressed as

$$\phi=AJ_n(Tr)+BN_n(Tr) \tag{34}$$

or as

$$\phi=AI_n(jTr)+BK_n(jTr) \tag{35}$$

depending on whether T^2 is larger or smaller than zero.

[9] A. W. Trivelpiece and R. W. Gould, J. Appl. Phys. 30, 1784 (1959).

J_n, N_n are Bessel functions of the first and second kind and I_n, K_n are modified Bessel functions of the first and second kind; all are of order n.

Originally, Trivelpiece and Gould[9] applied the solutions (34) and (35) to waves propagating in the x direction and standing in the θ direction. Now, the reverse situation is of interest. In the limit of $\omega_p/\omega_c\ll1$, and in the presence of slip in the θ direction, the equations of motion on which (32) to (35) are based reduce to

$$v_r=-(E_\theta/B)c,\quad v_\theta=(E_r/B)c,$$
$$v_z=-j(1/\omega)(e/m)E_z. \tag{36}$$

Then, expression (33) simplifies to

$$T^2=-k^2[1-(\omega_p^2/\omega^2)]. \tag{37}$$

In analogy to the linear case it is to be expected that ω is of the order of ω_p^2/ω_c and that T is therefore positive. Hence, solutions of the type given by (34) will be considered first.

In the empty spaces adjoining the charge sheet ω_p is zero, and the solutions to (32) can be expressed as

$$\phi=AI_n(kr)+BK_n(kr). \tag{38}$$

Differentiation of (34) and (38) with respect to r and θ yields the following field equations:

In space I,

$$E_\theta=(n/r)[A_II_n(kr)+B_IK_n(kr)],$$
$$E_r=j[A_II_n'(kr)+B_IK_n'(kr)]. \tag{39}$$

In space II,

$$E_\theta=(n/r)[A_{II}J_n(Tr)+B_{II}N_n(Tr)],$$
$$E_r=j[A_{II}J_n'(Tr)+B_{II}N_n'(Tr)]. \tag{40}$$

In space III,

$$E_\theta=(n/r)[A_{III}I_n(kr)+B_{III}K_n(kr)],$$
$$E_r=j[A_{III}I_n'(kr)+B_{III}K_n'(kr)], \tag{41}$$

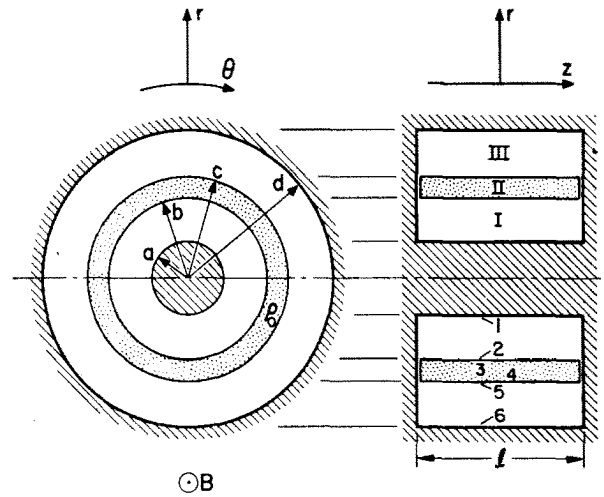

FIG. 6. Cylindrical sheet configuration of finite length with surrounding walls.

whereby the primes represent differentiations with respect to r, not Tr or kr, as is customary. These field components have to match at common boundaries. At surface 2, 3 one has

$$E_{\theta 3}=E_{\theta 2},$$
$$E_{r3}=E_{r2}+4\pi\sigma_3, \tag{42}$$

and similarly at surface 4,5

$$E_{\theta 5}=E_{\theta 4},$$
$$E_{r5}=E_{r4}+4\pi\sigma_4. \tag{43}$$

The surface charge densities σ_3 and σ_4 can be determined from

$$d\sigma/dt=v_r\rho_0, \tag{44}$$

which, together with the equations of motion (36), yield

$$4\pi\sigma_3=-j\frac{\omega_p^2}{\omega_c}\frac{E_{\theta 3}}{\omega-(n/b)u_3},$$
$$4\pi\sigma_4=j\frac{\omega_p^2}{\omega_c}\frac{E_{\theta 4}}{\omega-(n/c)u_4}. \tag{45}$$

Here, u_3 and u_4 are the slip velocities of the two surfaces.

Finally, at the conducting boundaries 1 and 6, the tangential field components must vanish.

$$E_{\theta 1}=0, \quad E_{\theta 6}=0. \tag{46}$$

By suitable manipulation of (39) through (46), one obtains a dispersion equation:

$$\frac{N_n(Tb)}{J_n(Tb)}\frac{b/n[F-N_n'(Tb)/N_n(Tb)][\omega-(n/b)u_3]-\omega_p^2/\omega_c}{b/n[F-J_n'(Tb)/J_n(Tb)][\omega-(n/b)u_3]-\omega_p^2/\omega_c}$$
$$=\frac{N_n(Tc)}{J_n(Tc)}\frac{c/n[G-N_n'(Tc)/N_n(Tc)][\omega-(n/c)u_4]-\omega_p^2/\omega_c}{c/n[G-J_n'(Tc)/J_n(Tc)][\omega-(n/c)u_4]-\omega_p^2/\omega_c}, \tag{47}$$

where

$$F=\frac{K_n(ka)I_n'(kb)-K_n'(kb)I_n(ka)}{K_n(ka)I_n(kb)-K_n(kb)I_n(ka)}$$
$$G=\frac{K_n(kd)I_n'(kc)-K_n'(kc)I_n(kd)}{K_n(kd)I_n(kc)-K_n(kc)I_n(kd)}.$$

Under the assumption that the sheet charges are unneutralized, the velocity slips u_3 and u_4 can be determined from

$$(\partial/\partial r)(rE_0)=4\pi\rho_0, \tag{48}$$

where E_0 is the field which results from the unperturbed sheet charges ρ_0. If (48) is combined with the equations of motion (36), and if u_3 is arbitrarily set to be zero (which establishes a frame of reference), one obtains

$$u_4=\tfrac{1}{2}(\omega_p^2/\omega_c)[c-(b^2/c)]. \tag{49}$$

For growth in time, ω may be now expressed as

$$\omega=(\omega_p^2/\omega_c)(\omega_r-j\alpha). \tag{50}$$

Introduction of (49) and (50) into (47) yields

$$[\tfrac{1}{4}\omega_r^2-\tfrac{1}{4}\omega_r(1-b^2/c^2)-j(\alpha/n)\omega_r+j(\alpha/2n)(1-b^2/c^2)$$
$$-\alpha^2/n^2]U-[\tfrac{1}{2}\omega_r-j(\alpha/n)]V$$
$$+[\tfrac{1}{2}(1-b^2/c^2)-\tfrac{1}{2}\omega_r+j(\alpha/n)]W+S=0, \tag{51}$$

where

$$U=bc\left\{S\left[F-\frac{N_n'(Tb)}{N_n(Tb)}\right]\left[G-\frac{J_n'(Tc)}{J_n(Tc)}\right]-\left[F-\frac{J_n'(Tb)}{J_n(Tb)}\right]\left[G-\frac{N_n'(Tc)}{N_n(Tc)}\right]\right\},$$

$$V=b\left\{S\left[F-\frac{N_n'(Tb)}{N_n(Tb)}\right]-\left[F-\frac{N_n'(Tb)}{N_n(Tb)}\right]\right\},$$

$$W=c\left\{S\left[G-\frac{J_n'(Tc)}{J_n(Tc)}\right]-\left[G-\frac{N_n'(Tc)}{N_n(Tc)}\right]\right\},$$

$$S=\frac{N_n(Tb)}{N_n(Tc)}\frac{J_n(Tc)}{J_n(Tb)}. \tag{52}$$

Real and imaginary parts of (52) can be separated into

$$[\tfrac{1}{4}\omega_r^2-\tfrac{1}{4}\omega_r(1-b^2/c^2)-\alpha^2/n^2]U$$
$$-\tfrac{1}{2}\omega_r V+\tfrac{1}{2}[(1-b^2/c^2)-\omega_r]W+S=0 \tag{53}$$

and

$$\omega_r=\tfrac{1}{2}(1-b^2/c^2)+(V+W)/U. \tag{54}$$

Elimination of ω_r finally yields the growth rate

$$\alpha=n\left\{\frac{S}{U}-\frac{1}{2}\left(1-\frac{b^2}{c^2}\right)\frac{V}{U}-\frac{1}{4}\left[\frac{1}{2}\left(1-\frac{b^2}{c^2}\right)-\frac{V+W}{U}\right]^2\right\}^{\frac{1}{2}}. \tag{55}$$

Since (55) depends on k and T, values for α can be secured only by solving simultaneously (55) and

$$T^2\cong-k^2\left(1-\frac{\omega_c^2/\omega_p^2}{\omega_r^2}\right), \tag{56}$$

where ω is approximated by ω_r.

Because of the complicated dependence of (55) on T, this appears to be possible only with the help of computers. However, in a number of special cases of practical interest, analytic solutions for α may be secured directly, as is shown below.

The complication in (55) is associated with the z-directed component of motion. In some configurations v_z can be considered negligibly small. In that case, T becomes equal to jk [according to (36)] and the solution within the sheet is described by (38). All Bessel functions then are of the second kind, and (55) can give values for α directly.

The situation simplifies further when the conducting center rod is eliminated. This applies to most plasma and discharge configurations, and with $a=0$, α can be expressed as

$$\alpha=n\{-\tfrac{1}{4}[\tfrac{1}{2}(1-b^2/c^2)-A-B]^2 -\tfrac{1}{2}(1-b^2/c^2)A+AC\}^{\frac{1}{2}}, \quad (57)$$

where

$$A=[I_n(kc)/I_n(kd)][K_n(kd)I_n(kc)-K_n(kc)I_n(kd)],$$
$$B=[I_n(kb)/I_n(kd)][K_n(kb)I_n(kd)-K_n(kd)I_n(kd)],$$
$$C=[I_n(kb)/I_n(kc)][K_n(kb)I_n(kc)-K_n(kc)I_n(kb)].$$

A computer was utilized to evaluate (57) for growth rates over a wide range of conditions. In Figs. 7, 8, and 9 values for α are presented as a function of the normalized inner sheet radius b/c with the outer sheet radius c held constant. The character of the growth dependence on sheet width is generally similar to that obtained for the flat sheet.[4] In detail, the growth curves for the circular case vary substantially with proximity of walls (Fig. 7), with number of wavelengths around the circumference (Fig. 8), and with wavelength in the z direction (Fig. 9). In one respect, linear and circular cases are significantly different; in the circular configuration the wavelength cannot exceed the circumference. Hence, each circular geometry possesses a maximum sheet width up to which growth can take place. Sheets of larger widths should be stable (at least in the limit $\omega_p/\omega_c \ll 1$). The critical width at which growth begins is of particular interest for practical purposes and it is therefore presented for various geometries in Fig. 10.

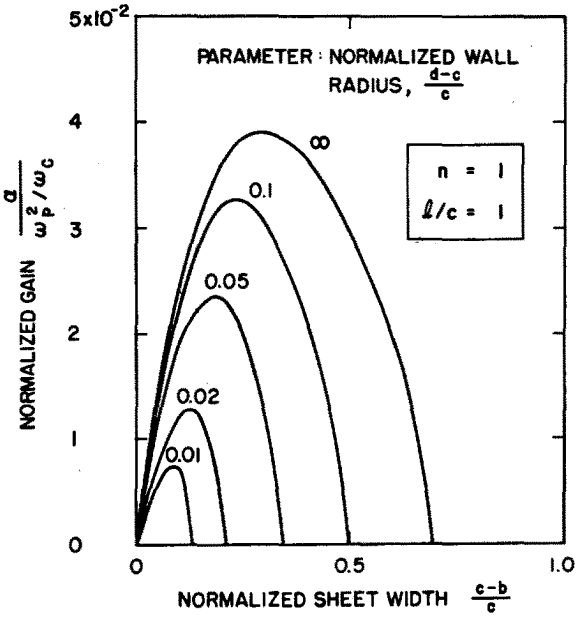

FIG. 7. Growth rates in a cylindrical sheet configuration as a function of the sheet thickness, with outer wall radius as parameter. Inner wall radius $a=0$, length of the cylinder $l=c$, order of the circumferential mode $n=1$.

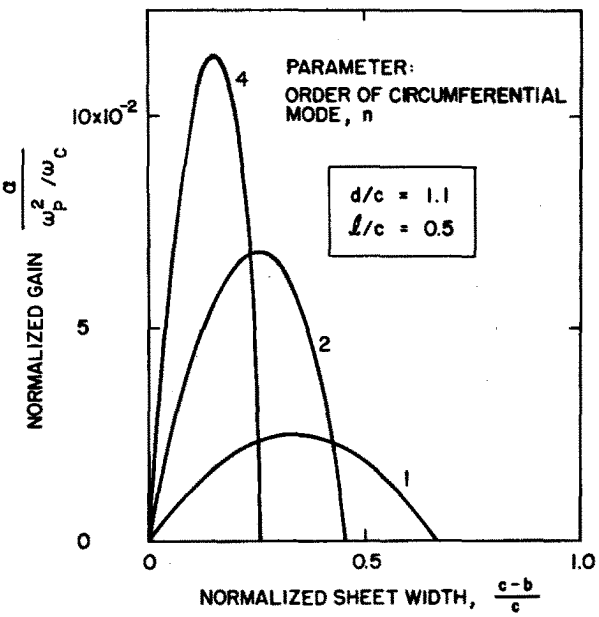

FIG. 8. Growth rates in a cylindrical sheet as a function of sheet thickness, with order of the circumferential mode as parameter. Inner wall radius $a=0$, outer wall radius $d=1.1c$, length of the cylinder $l=0.5c$.

For configurations which are long in the z direction,[10] the Bessel functions in (57) convert into exponential expressions as

$$I_n(kr) \rightarrow (kr/2)^n 1/n!,$$
$$K_n(kr) \rightarrow (2/kr)^n (n-1)!/2,$$

and α becomes

$$\alpha=n\{-\tfrac{1}{4}[\tfrac{1}{2}(1-b^2/c^2)+(1/2n)(1-[c/d]^{2n}) -(1/2n)(1-[b/d]^{2n})]^2 +(1/4n)(1-b^2/c^2)(1-[c/d]^{2n}) -(1/4n^2)(1-[b/c]^{2n})(1-[c/d]^{2n})\}^{\frac{1}{2}}. \quad (58)$$

An interesting property of this solution is that the fundamental mode for which $n=1$ is generally stable. In this case, the second and third terms in (58) cancel out and α must be zero or imaginary. Physically this can be attributed to insufficient velocity slip resulting from a combination of radial dispersion of the space charge fields and the proportional increase in tangential velocity with radius for a given rotation frequency. As a result, the two surface waves cannot become

[10] This case has been treated recently also by R. H. Levy, Phys. Fluids 8, 1288 (1965).

synchronized or, in the limit of an infinitely removed wall cylinder ($d=\infty$) can just synchronize but cannot produce gain. It should be added that in some configurations where a conducting center conductor is present ($a\neq 0$), the fundamental wave mode does grow, since here the velocity slip can again be sufficiently large. Furthermore, if the fundamental mode is unstable, it produces lateral displacements of the cylindrical sheet surfaces against each other. Thus, the charge sheet becomes deformed into a "lobsided" cylinder.

Finally, the linear case is approached when n in (58) is permitted to go to infinity. Then

$$(c/d)^{2n}\rightarrow e^{-2\beta\delta}$$
$$\tfrac{1}{4}n[1-(b^2/c^2)]\rightarrow\tfrac{1}{2}\beta t,$$

where

$$n/c=\beta,$$
$$\delta=d-c,$$
$$t=c-b.$$

This leads to

$$\alpha=\{-\tfrac{1}{4}[\beta t-\tfrac{1}{2}(1-e^{-2\beta t})e^{-2\beta\delta}]^2+\tfrac{1}{2}\beta t(1-e^{-2\beta\delta})-\tfrac{1}{4}(1-e^{-2\beta t})(1-e^{-2\beta\delta})\}^{\frac{1}{2}} \quad (59)$$

and in the limit $\delta\rightarrow\infty$,

$$\alpha=[-\tfrac{1}{4}(\beta t)^2+\tfrac{1}{4}\beta t-\tfrac{1}{2}(1-e^{-2\beta t})]^{\frac{1}{2}}, \quad (60)$$

which is equivalent to Gould's expression and identical to the earlier derived (30). Values of α obtained from (59) and (60) are presented in Fig. 11.

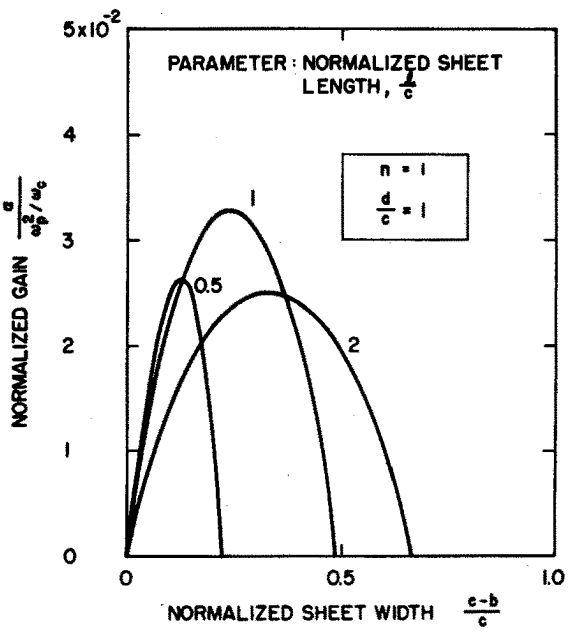

FIG. 9. Growth rates in a cylindrical sheet as a function of sheet thickness, with sheet length as parameter. Inner wall radius $a=0$, outer wall radius $d=1.1c$, circumferential order $n=1$.

IV. APPLICATION TO ACTUAL CONFIGURATIONS

In this final section, the applicability of the described theoretical models to several plasma, discharge, and electron device configurations is discussed briefly. One such configuration is the sheath of a magnetically confined plasma column. At first sight it would appear as if the plasma sheath could not satisfy the basic requirement of having two free surfaces. Indeed, the charges composing the sheath extend from within the plasma up to the sheath surface. However, a second surface is provided by charges of opposite polarity; these fill the plasma up to the inner edge of the sheath (see Fig. 12). If the condition $\omega_p/\omega_c\ll 1$ is fulfilled for both charge species, the instability analysis will be identical to the analysis given for a single component charge sheet. This can be seen immediately from the continuity Eq. (44) where $d\sigma/dt$ remains unchanged when the polarity of the charge density ρ_0 and the direction of the surface density gradient are reversed.

Plasma columns often are long and thin; if this is the case, the stability (or instability, as the case may be) can be determined from (58) which applies to infinitely long wavelengths in the z direction. Accordingly, it is expected that the fundamental mode will be stable. However, since most sheaths are quite narrow, it is likely that some of the higher order modes are excited.

A second configuration to be considered is the low-pressure reflex discharge. This mode is characterized by a circular electron layer which lines the inside of the anode cylinder and which constitutes the active portion of the discharge. Typical configurations of this discharge mode (in ion pumps, ionization gauges, and ion sources) are short in the z direction. Equation (57) gives growth rates for short sheets and would apply here, provided it could be shown that v_z is negligible.

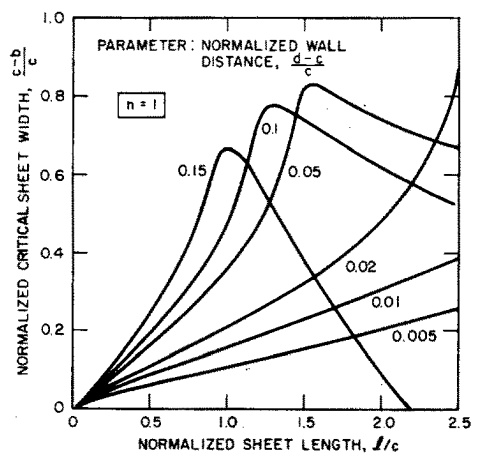

FIG. 10. Critical sheet thickness as a function of the sheet length, with wall distance as parameter. The sheets are stable above and unstable below the curves shown. The order of the circumferential mode is $n=1$.

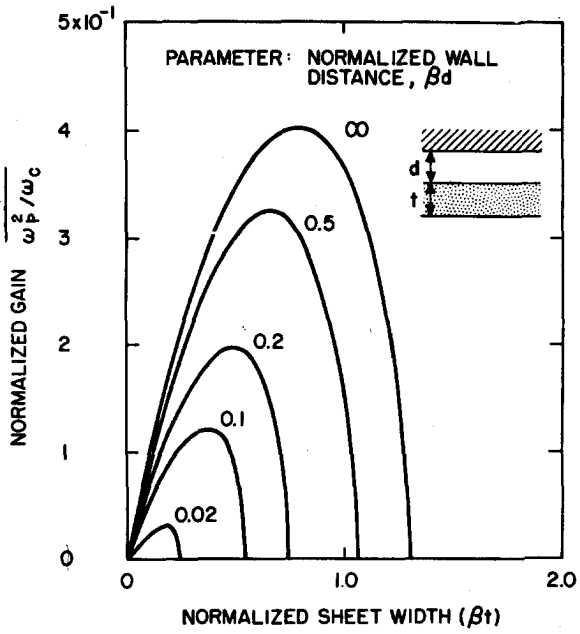

FIG. 11. Growth rates of a linear sheet as a function of sheet width with distance d from a parallel wall as parameter.

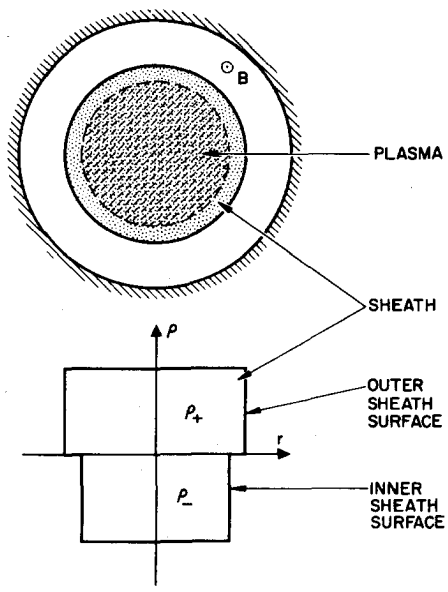

FIG. 12. Cylindrical plasma configuration. The two surfaces required for the diocotron interaction are provided by the inner and outer sheath surfaces.

Typical densities in the electron layer of reflex discharges are of the order of 10^{10} particles/cm^2. The geometrically reduced plasma frequency in a discharge chamber 2 cm in diameter and 2 cm long, for example, can be expected to be 200 to 400 Mc/sec depending upon the exact shape of the electron layer. The average electron energy in these discharges is of the order of hundreds of electron volts, and, accordingly, the average velocity is close to 10^9 cm/sec. Thus, most electron cross the length of the discharge chamber several times during a single oscillation cycle. All z-directed acceleration due to the wave fields should therefore be nearly canceled out. Hence, $v_z \cong 0$, and (57) which applies to short sheet configurations may be utilized.

In the third and last configuration to be discussed, the classical magnetron geometry, a circular electron stream of short axial length is enclosed between two concentric wall cylinders. Magnetrons may be divided into two classes with respect to the instability in question. In the first, electrons are emitted from the inner cylinder; in the second, electrons are released from a separate, axially displaced cathode. The electron cloud of the first type extends outward from the inner electrode with a density distribution which is likely to taper off with radius. Hence, only a single, free electronic surface exists and the diocotron effect should not occur.

In the second case, the electrons are launched axially and enter the interaction region as a hollow beam. It is unlikely that this beam completely fills the space between both wall cylinders and, as a result, unstable growth is conceivable. For a detailed analysis, one has to resort to (55), but matters can again be simplified by taking $T=jk$. This appears to be permissible since again the axial transit time through the interaction region is short in comparison with the geometrically modified plasma frequency period.

To determine whether the diocotron effect actually occurs in the configurations discussed above, experiments have been initiated and are being carried out at this laboratory. Results obtained to data confirm the presence of the instability in all three configurations. A detailed account of this experimental work will be published in the near future.[11]

ACKNOWLEDGMENTS

The author acknowledges stimulating discussions with R. C. Knechtli, A. Fafarman, and R. L. Poeschel, of the Hughes Research Laboratories, and is indebted to G. Guss, also of the Hughes Research Laboratories, for performing the computer work.

[11] L. J. Knauer and R. L. Poeschel, Proc. 7th Intern. Conf. on Phenomena in Ionized Gases, Belgrade, 1965.